Materials Horizons

Relating Reorganization Energies, Exciton Diffusion Length and Non-Radiative Recombination to the Room Temperature UV-Vis Absorption Spectra of NF-SMA

Journal:	*Materials Horizons*
Manuscript ID	MH-COM-10-2022-001228.R1
Article Type:	Communication
Date Submitted by the Author:	14-Nov-2022
Complete List of Authors:	kashani, Somayeh; North Carolina State University at Raleigh, Physics; North Carolina State University at Raleigh, Organic and Carbon Electronics Laboratories (ORaCEL) Wang, Zhen; North Carolina State University, Department of Physics; North Carolina State University, Organic and Carbon Electronics Laboratories (ORaCEL) Risko, Chad; University of Kentucky, Chemistry; University of Kentucky, Center for Applied Energy Research (CAER) Ade, Harald; North Carolina State University, Physics; North Carolina State University at Raleigh, Organic and Carbon Electronics Laboratories (ORaCEL)

New Concepts

We systematically analyze the room temperature (RT) UV-Vis absorption spectra for electron-accepting molecules envisioned to replace fullerenes as electron transport materials in organic solar cells, and categorize them based on their molecular structures, intramolecular reorganization energies, and conformational uniformities as determined by multiparameter Franck Condon analyses of their RT absorption spectra. We show that MFC fitting allows accurate determination of the reorganization energies, which can be utilized as a predictive measure for exciton diffusion length and non-radiative voltage losses of the organic semiconductor in a solar cell. The MFC results show that Y6 and like-derivatives exhibit very small intramolecular relaxation energies and high conformational uniformity in solution. We also demonstrate that RT UV-Vis analyses are experimentally much simpler than complementary measurements of reorganization energies, and thus a tool of great utility. Moreover, the good agreement between experiment and density functional theory (DFT) calculations show that the latter can be used to design molecules in-silico with low relaxation energies and single conformations with the aim of limiting energetic disorder.

COMMUNICATION

Relating Reorganization Energies, Exciton Diffusion Length and Non-Radiative Recombination to the Room Temperature UV-Vis Absorption Spectra of NF-SMA

Received 00th January 20xx,
Accepted 00th January 20xx

DOI: 10.1039/x0xx00000x

Somayeh Kashani,[a] Zhen Wang [a], Chad Risko[b] and Harald Ade*[a]

Understanding excited-state reorganization energies, exciton diffusion lengths and non-radiative (NR) recombination and the overall optoelectronic responses of nonfullerene small molecule acceptors (NF-SMAs) is important in order to rationally design new materials with controlled properties. While the effects of structural modifications on the optical gaps and electron affinities of NF-SMAs have been studied extensively, analyses of their absorption spectra that carefully characterize electronic and vibrational contributions to allow comparisons of reorganization energies and their implications for exciton diffusion lengths and NR recombination have yet to be reported. Here, we study the room temperature absorption spectra of three structural classes of NF-SMAs in dilute solutions through multiparameter Franck Condon (MFC) analyses and density functional theory (DFT) calculations. We show that the absorption spectra of these NF-SMAs can be categorized based on molecular structure–spectra correlation. The absorption spectra of curved, Y6-like structures can be described using an MFC model with two electronic transitions and two effective vibrational modes. The results of MFC/DFT analyses reveal that Y6 exhibits the smallest intra-molecular reorganization energy among the materials studied. Linear ITIC-like molecular structures reveal larger reorganization energies and reduced conformational uniformity compared to Y6. Meanwhile structures such as EH-IDTBR, which have an extra π-conjugated moiety between the donor and acceptor moieties, have large excited-state reorganization energies and low degrees of conformational uniformity. Since the intra-molecular reorganization energy is correlated with exciton diffusion length and nonradiative voltage losses (ΔV_{nr}), our results highlight the power of RT absorption spectroscopy and DFT calculations as simple tools to designing improved OSCs materials with small reorganization energies, small ΔV_{nr}, large exciton diffusion length and low energetic disorder (due to a strongly dominant conformation).

1. Introduction

State-of-the-art organic solar cells (OSCs) rely on bulk-heterojunction (BHJ) active layers utilizing non-fullerene small molecule acceptors (NF-SMAs) and polymer donors. Since the initial report of ITIC by Zhan et al. in 2015[1], the efficiencies of single-junction OSCs have reached over 19% thanks in part to the rapid development of ladder-type, fused-ring cores with promising properties that can be tuned through molecular engineering[2–7]. A wide range of NF-SMAs have been developed by using different acceptor (A) or donor (D) building blocks in the core, introducing different types of π-bridges between the A end-group and the D core. Side-chain modifications are used to manipulate the electronic and optical properties of these materials and their thin film manifestations, which are impacted by molecular packing that controls optical and electronic molecular coupling[8–15]. The device-relevant thin film properties are generally correlated to the intrinsic molecular properties. Among these properties, small reorganization energies and electronic disorder due to structural/conformational disorder are of great importance to achieving high performance through small voltage losses[16–18]. Thus, understanding the intrinsic molecular reorganization energy and conformation populations is of great importance in order to provide molecular design guidelines that can lead to desirable bulk properties with large exciton diffusion length and low nonradiative voltage losses (ΔV_{nr}).

[a] Department of Physics and Organic and Carbon Electronics Laboratories (ORaCEL), North Carolina. E-mail: hwade@ncsu.edu
[b] Department of Chemistry and Center for Applied Energy Research (CAER), University of Kentucky, Lexington, Kentucky 40506, USA.
† Footnotes relating to the title and/or authors should appear here.
Electronic Supplementary Information (ESI) available: [details of any supplementary information available should be included here]. See DOI: 10.1039/x0xx00000x

Measurements of reorganization energies and energic disorder are often performed through specialized high sensitivity photocurrent measurements or assessed through simulations and modeling[19–27]. Optical absorption spectroscopy is a complementary method that is often a convenient and common probe to study the opto-electronic properties of materials,[28] and can provide information about structure-related properties such as the reorganization energies[29,30], conformational diversity[31–33] in thin films or solutions, order-disorder ratios and aggregation[15,34–40]. Absorption and emission spectra of organic molecules and polymers can feature vibrational progressions due to the electron–phonon coupling that can be described by Franck-Condon (FC) models[38,41]. However, the shape (peak ratios, peak to peak spacing and broadening) of absorption and emission spectra of an ensemble of molecules in dilute solution can also be influenced by other parameters including conformational uniformity, multiple electronic transitions, as well as possible aggregate states. Hence, simple FC models often fail to describe the absorption spectra of a solution, even in very low concentrations. Thus, detailed temperature-dependent spectroscopy in both the absorption and emission channels are often utilized to disentangle various contributions, particularly aggregation. Low temperature studies often probe aggregates that are not present at reduced concentrations at higher temperatures but related to spectra in a solid thin film. Frequently, spectral features in absorption or photoluminescence spectra of solutions or solid films acquired at room temperature (RT) are modeled as single electronic transition and a dominant FC vibrational progression with 0-0, 0-1, and 0-2 labels for the transitions. However, the use of single FC models are not always correct due to the presence of multiple FC or even non-FC contributing parameters. Different scenarios are conceptualized in **Figure 1**. In the simplest case, the absorption spectrum is a vibrational progression of a single electronic transition with one dominant vibrational mode (**Figure 1-a**). In contrast, the presence of more than one dominant vibrational mode (**Figure 1-b**), or contribution from higher electronic transitions, leads to more complex absorption spectra (**Figure 1-c**). Also, the coexistence of different conformation populations results in even more complex contributions and broadened, apparently simpler absorption spectrum due to the superposition of all the contributing species (**Figure 1-d**). Without properly disentangling contributions to RT UV-vis spectra, their utility to measure reorganization energies λ_{re} and conformation distribution in NFAs and to infer the related consequences such exciton diffusion length and low ΔV_{nr} and electronic disorder, respectively, is limited.

Here, utilizing multi-parameter FC (MFC) analysis of absorption spectra of NF-SMAs in dilute solutions in combination with density functional theory (DFT) / time-dependent DFT (TD-DFT) calculations, we unravel correlations between the absorption spectra of SM-NFAs, their molecular structures, reorganization energy, and conformation populations. We specifically endeavor to use only RT spectra to delineate the utility of FC analysis when supported by DFT calculations in the most common, i.e., at RT, use of UV-vis

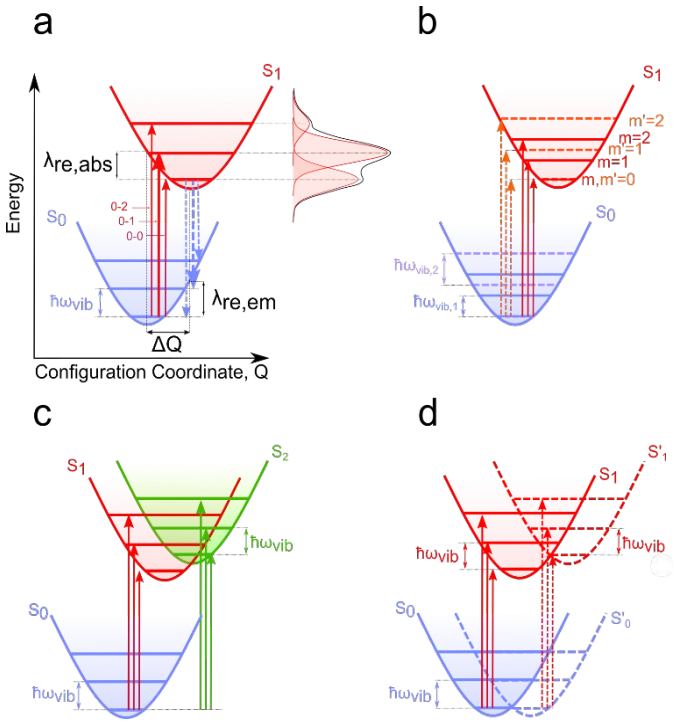

Figure 1 Potential Energy diagram as a function of configuration coordinate Q, which is related to the reorganization energies $\lambda_{re,abs}$, $\lambda_{re,em}$, illustrating possible contributions in absorption spectra in the single molecule regime for: (a) Simple model with one electronic transition from ground state: S_0 (blue) to first singlet excited state: S_1 (red), and one effective vibrational mode ($\hbar\omega_{vib}$). $I_{0\text{-}m}$ are the probability of transitions from 0^{th} vibrational level of ground state to the m^{th} overtone in the excited state. The most probable transitions in the absorption or emission processes, i.e., with the largest overlaps, are shown with ticker arrows. The absorption spectrum corresponding to this model is shown on the top right corner. (b) One electronic transition ($S_0 \rightarrow S_1$) and two effective vibrational modes: $\hbar\omega_{vib,1}$ with dark blue (red) solid lines and $\hbar\omega_{vib,2}$ with light blue (orange) dashed lines in S_0 (S_1) state. (c) A single molecule with two electronic contributions $S_0 \rightarrow S_1(\text{red})$ and $S_0 \rightarrow S_2(\text{green})$ and one dominant vibrational mode ($\hbar\omega_{vib}$). (d) A system with two coexisting conformations that have different electronic states (solid and dashed lines) and one effective vibrational mode ($\hbar\omega_{vib}$).

spectroscopy. We show that incorporating an MFC model that considers all the contributions to an RT absorption spectrum provides information about the reorganization energy and conformational diversity for NF-SMAs and reveals a molecular structure-property relation. Specifically, for the case of Y6, the result of the MFC analysis confirms the reported small reorganization energy compared to the other NF-SMAs and a single conformation which should lead to small energic disorder. The success of Y6 in state-of-the-art OSCs can be attributed at least partially to these two important characteristics as they result in larger exciton diffusion length and smaller non radiative (NR) voltage losses in OSCs.

2. Methods

2.1 Material selections

To study the absorption spectra of NF-SMAs and address the effect of different molecular structures on their reorganization energy and degree of conformation uniformity, we examined NF-SMAs with different chemical structures that could be grouped into three different sets based on their molecular structures (**Figure 2**). The first group, representing ITIC-like

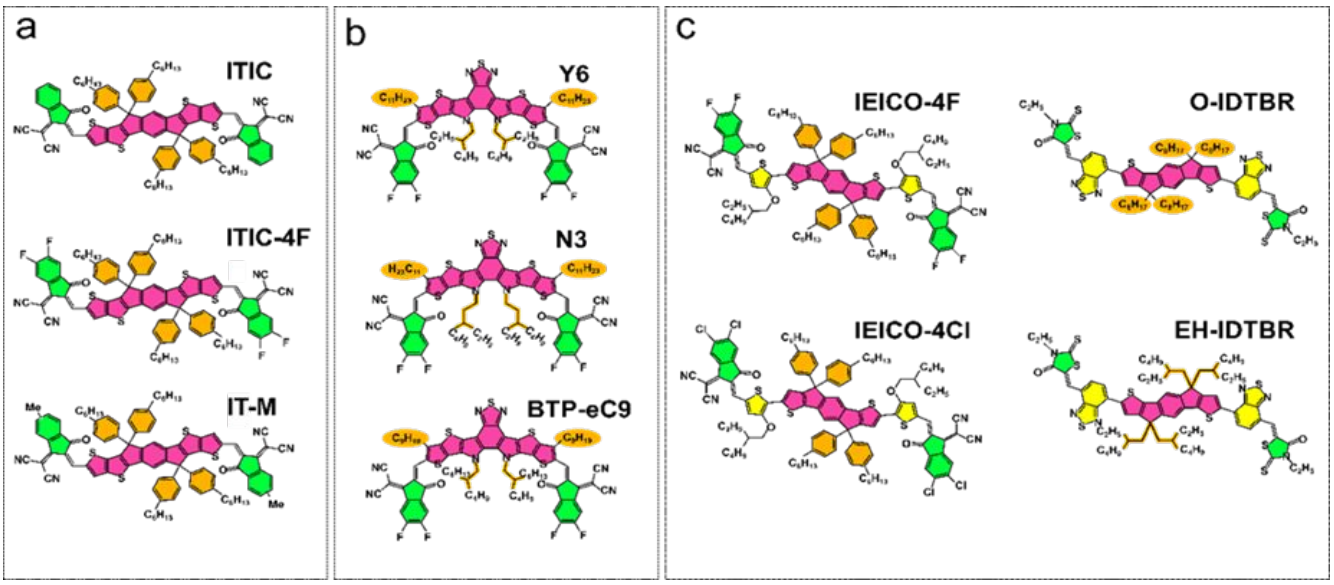

Figure 2 Molecular structure of different type of NA-SMAs studied in this study. (a) ITIC-like structures, (b) curved Y6-like structures and (c) EH-IDTBR-like SMAs with A-π-D-π-A structure.

molecules, have acceptor-donor-acceptor (A-D-A) structures with indacenodithiophene (IDT) as the donor core unit with a rigid and coplanar geometry (**Figure 2-a**). IDT-based NF-SMA in this group are capped with indanone end group for ITIC or chemically modified indanone for ITIC-4F and IT-M as shown in **Figure 2-aError! Reference source not found.**[42,43]. The second class are Y6-like SMAs with curved shapes (**Figure 2-b**), used in many state-of-the-art, high performance OSCs[7,44–46]. Y6, N3 and BTP-eC9 belong to this group. These molecules have acceptor–donor–acceptor–donor–acceptor (A–DA'D–A) structures where the electron-deficient benzothiadiazole (BT) capped with more extended π-conjugated thieno[3,2-b] thiophene (TT) constitutes a DA'D ''push–pull'' fused core, endowing it with good planarity and narrow bandgap. The conformation of Y6-like structures are considered locked into the curved shape [47–49]. In the third group of SMAs, a conjugated π-bridge is inserted between the D unit and A units to form A-π-D-π-A structure SMAs (**Figure 2-c**). IEICO-4F, IEICO-4Cl, O-IDTBR and EH-IDTRB are in this group. The bridge incorporated between D and A units results in extended conjugation length and a red shift in the absorption spectra; however, this extra moiety decreases the rigidity of the molecule and affects the conformational diversity, optoelectronic, electrochemical, and packing properties[50,51]. The full chemical names of the molecules are provided in **SI 1.**

2.2 Experiments

Solutions of different NF-SMA were prepared in chloroform (CF) at 0.02mg/ml concentration. The UV-vis absorption spectra of different samples were recorded using a Cary 50 spectrophotometer. The photoluminescence (PL) spectra were carried out with a Fluorometer FLS 980.

2.3 Simulations

The electronic and optical properties of the NF-SMAs were determined through density functional theory (DFT) and time-dependent DFT (TD-DFT), respectively. Vertical absorption calculation was performed by TD-DFT energy calculation on the ground state geometry for different functional. The vertical emission calculation was performed by TD-DFT optimization of first excited state geometry following with a TD-DFT energy calculation. The side chains are replaced by methyl groups to reduce the computational time unless stated otherwise. Solvent effects were taken into account using the Polarizable Continuum Model (PCM) model[52–55] for CF. Three different functionals were used in the study – B3LYP, PBE0, ωB97X-D – in combination with the 6-31G(d,p) basis set. B3LYP/6-31G(d,p) and ωB97X-D/6-31G(d,p) achieve better agreement than PBE0/6-31G(d,p) with the experimental values for $\varepsilon_{S_0 \rightarrow S_1}$ and $\varepsilon_{S_0 \rightarrow S_2}$derived from FC analysis. In the main manuscript, we only report DFT/TDDFT results at the B3LYP/6-31G(d,p) level since its prediction of Stokes shift and reorganization energy is closer to the values derived from FC analyses. Comparison between calculation results using different functionals are provided in the Supplementary Information (SI) in **SI 3**.

3. Results

Figures 3a-c show the optimized geometry of a representative molecule of each group, i.e., ITIC, Y6 and EH-IDTBR, in their ground states, as well as the TDMs of the three lowest transitions, while **Figures 3d-f** show calculated relaxed dihedral potential energy surface (PES) scans for ITIC, Y6 and EH-IDTBR, all at the B3LYP/6-31G(d,p) level of theory. Energy scans were performed by constraining the dihedral angle at a given angle and allowing the rest of the structure to relax. The horizontal axes are normalized with respect to the dihedral angle of the optimized geometry (Φ_{opt}). The PES of Y6 (**Figures 3-e**) features with one global minimum (GM) at $\Phi_{opt} = 179.8°$ and a local minimum (LM) at $\Phi - \Phi_{opt} = 150°$ with a 250 meV potential

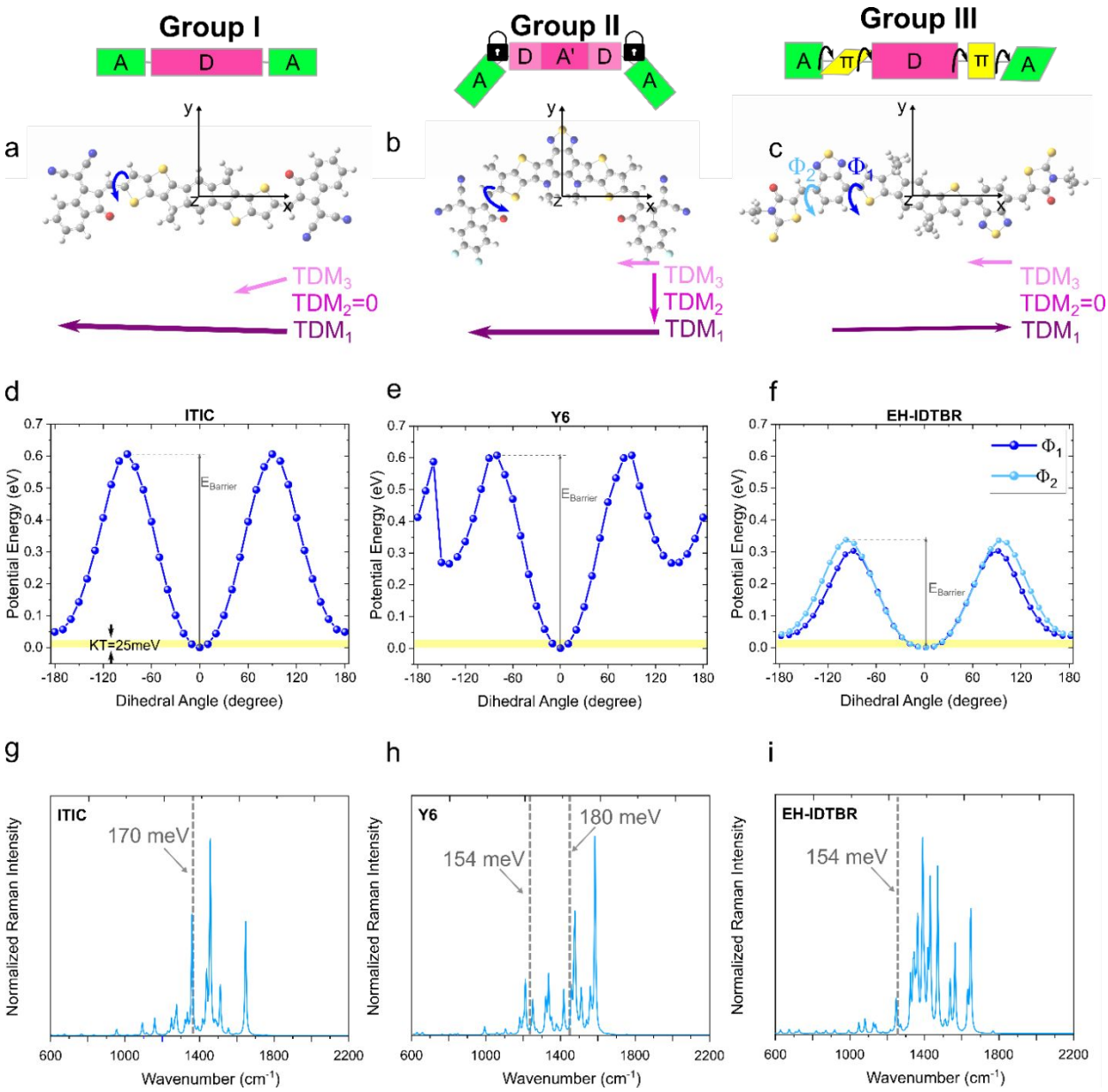

Figure 3 Optimized geometry of (a) ITIC, (b) Y6 and (c) EH-IDTBR. Transition Dipole Moments (TDM) for the first three electronic transitions are shown below each of the molecular structures and are accurately portrait relative to the x- and y-axis. The calculated Potential energy scan as a function of dihedral angles for ITIC (d), Y6 (e) and EH-IDTBR (f). Simulated Raman Spectra of ITIC (g), Y6 (h) and EH-IDTBR (i). Calculation were performed in gas phase using DFT at the B3LYP level of theory with a basis set of 6-31G(d,p). The dashed gray lines indicate the effective vibrational mode derived from FC analyses of experimental data.

energy difference with respect to the GM. Using Boltzmann distribution (**SI 2**) at room temperature, the population ratio corresponding to these angles is 0.005%, suggesting that only the global minimum of Y6 is thermodynamically preferred, as previously discussed by Wu et al[56]. The potential barriers ($E_{barrier}$) is another determining factor as it controls the rate of interconversion process between two conformational states in the solution. This rate can be changed by increasing the temperature ($k \propto \exp\left(-\frac{\mathrm{E_{barrier}}}{k_B T}\right)$). But, when the system is in equilibrium at a fixed temperature (here RT), Boltzmann distributions describe the probability that molecules in the solution will be in a certain conformational state. ITIC and Y6 both have similar $\mathrm{E_{barrier}} \approx 600\, meV$, and indeed similar transition rates between conformations. However, the energy difference between GM and LM is 250 meV for the case of Y6, and 50 meV for ITIC (**Figures 3Error! Reference source not found.-d** and **e**). This indicates that in equilibrium in solution at RT, ITIC has less conformation uniformity with two conformers coexist with a population of 85% and 15%, for GM and LM respectively.

The presence of the additional π-moieties in EH-IDTBR present two torsion angles, Φ_1 and Φ_2, for consideration, and, hence, more degrees of freedom. The $E_{barrier}$ for both dihedral angles are smaller compared to the ITIC and Y6 (**Figure 3-f**), which means higher interconversion rate between conformational at elevated temperatures. The energy difference between GM (Φ_1, Φ_2=0°) and LM (Φ_1, Φ_2=180°) for

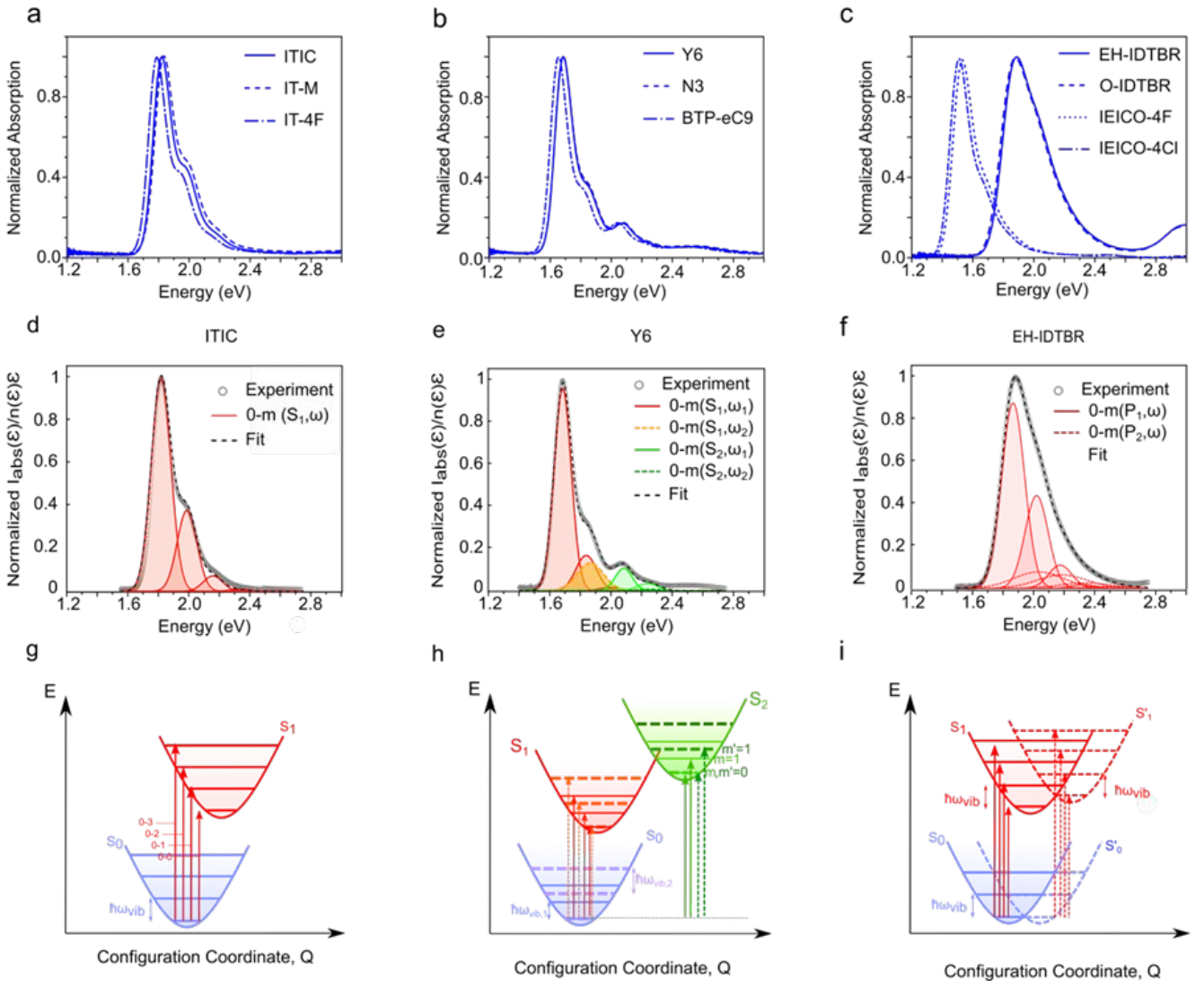

Figure 4 Normalized Jacobian corrected absorption spectra of (a) ITIC-like, (b) curved Y6-like and (c) EH-IDTBR-like NF-SMAs in CF solution (0.02mg/ml). The best FC model fitted (dashed black lines) to the Normalized absorption spectra after both Jacobian and photon DOS corrections (gray open circles) for (d) ITIC, (e) Y6 and (f) EH-IDTBR. The fitting line is sum of Gaussian peaks corresponding to the different $I_{0\text{-}m}$ transitions from ground state S_0 to S_1red,orange) or S_2(green,blue). (b) Schematic potential energy diagram derived from FC analysis for (g) ITIC, (h) Y6 and (i) EH-IDTBR.

both PES dihedral scans is comparable to the thermal energy at RT of 26 meV, resulting in a population ratio of 20% and 25% based on Boltzmann distribution. Thus, EH-IDTBR has the lowest degree of conformational rigidity with nearly equal probability of all four possible conformations for each π-bridge.

We determined the first three singlet excited states using DFT/TD-DFT calculations with 6-31G(d,p) basis set considering CF as the solvent. In **Figures 3a-c**, the transition dipole moments (TDM) for the first three singlet excited states are shown along with the optimized geometry of the molecule. The first electronic transition (determined at the B3LYP/6-31G(d,p) level of theory) for ITIC occurs at energy $\varepsilon_{S_0\rightarrow S_1} = 1.77$ eV with the TDM_1 vector aligned along the long axis of the π-conjugated backbone, while the TDM_2 is zero. The third electronic excitation of ITIC is at $\varepsilon_{S_0\rightarrow S_3} = 2.53$ eV with TDM_3 having components along the long and short axes of the backbone. For the case of Y6, the first and second electronic transitions are allowed with energies equal to $\varepsilon_{S_0\rightarrow S_1} = 1.71$eV and $\varepsilon_{S_0\rightarrow S_2} = 2.05$ eV, and with TDM vectors along the long and short axis of the molecular structure, respectively. The third electronic transition is also allowed with energy $\varepsilon_{S_0\rightarrow S_3} = 2.75$ eV and TDM_3 along the backbone. The calculated energy for the $\varepsilon_{S_0\rightarrow S_1}$ transition for EH-IDTBR is at 1.58 eV while the second electronic transition is not allowed (zero TDM). The third electronic transition is also allowed with energy $\varepsilon_{S_0\rightarrow S_3} = 2.42$ eV and TDM_3 along the backbone. More details about the excited state properties determined with different functionals are provided in **SI 3.**

We also simulate the NF-SMA vibrational modes in CF to understand the possible impact of vibrations on the RT spectra. Due to the dipole moment selection rules, in photon absorption a dipole change due to the vibrational mode is not allowed and thus only Raman modes can couple to the absorption. **Figures 3g-i** show the simulated Raman spectra of ITIC, Y6 and EH-IDTBR

in the CF in blue solid line. The effective vibrational energy derived from FC analysis of experimental data are also shown in gray dashed lines. Simulated Raman spectra for ITIC feature five strong lines, Y6 has eight strong lines and EH-IDTBR has two well-resolved features at 1651 cm^{-1} (205 meV), 1568 cm^{-1} (194 meV) and multiple peaks at ~1400 cm^{-1}(174 meV). If the measured spectra are sufficiently well resolved, all these normal modes and their overtones could be identified separately, however due to heterogeneous broadening effects, only one or a few effective modes and their mean energies can be observed[41]. As we will discuss later, FC analysis can be used to investigate the number of contributing effective modes and how it is correlated with the structure properties and conformation uniformity.

Figures 4a-c show the normalized Jacobian- and photon density of states (DOS) corrected absorption spectra of the NF-SMAs in CF at low concentrations (0.02 mg/ml). The experimental details on solution preparation and measurement are discussed in the experimental methods (**SI 1**). The simple FC model and all the required spectral corrections, including Jacobian and DOS, are explained in **SI 4**. As shown in **Figures 4-a**, the absorption of ITIC-like SMAs in solution features three successive peaks. For the case of ITIC, the absorption spectrum in solution exhibits its first peak at 1.82 eV and further vibronic replicas at 1.98 eV and 2.15 eV. The energy of the first peak is comparable to the $\varepsilon_{S_0 \to S_1} = 1.77\text{eV}$ determined using DFT/TD-DFT at the B3LYP 6-31(d,p) level of theory. The energy difference between two successive peaks for this group is approximately 160 meV (equally "distanced" from each other), which is very close to reported values for the vibrational quanta of the effective (dominant) vibrational mode in most organic oligomers/polymers[41]. **Figure 4-b** shows the absorption spectra for Y6-like structures in solution. In contrast to the ITIC-like NF-SMAs, the absorption spectra of curved structures feature three apparent main peaks/shoulders that are not equally spaced from each other, located at 1.69, 1.84 and 2.08 eV. DFT/TDFT computations for electronic transitions yield $\varepsilon_{S_0 \to S_1} = 1.71\text{eV}$ and $\varepsilon_{S_0 \to S_2} = 2.05\ \text{eV}$ which are comparable to the first and third peak in the absorption. The energy difference between the first two peaks is 150 meV, while the difference between the second and third peak is 240 meV. These observations indicate that a simple FC model with only one electronic transition and one dominant vibration mode is not able to predict the absorption spectra of this group. As shown in **Figure 4-c**, the absorption spectra of the third group of molecular structures feature a broad, asymmetric peak with no obvious vibrational replica; EH-IDTBR in solution, for instance, has one broad peak at 1.89 eV, with a small shoulder at 2.04 eV. As we discuss below, applying FC analysis for the case of EH-IDTBR is quite challenging due to the lack of obvious vibrational replica in the absorption spectra.

Figures 4d-f show the normalized absorption spectra of ITIC, Y6 and EH-IDTBR in CF after both Jacobian and photon DOS corrections (gray open circles) and the best model fit to the experimental data (dashed black lines). It should be noted that the refractive index of CF can be considered as a constant within the visible range of the spectrum[57] for the purpose of photon DOS corrections. In **Figures 4g-i**, schematic energy diagrams derived from FC analyses for each group are illustrated. A simple FC model for a population undergoing an electronic transition ($S_0 \to S_1$) with one effective vibrational mode and 4 overtones (red arrows) can satisfactorily describe the absorption spectra of ITIC in a dilute solution. Different 0-m overtones, with m=0,1,2,3 are shown with red Gaussian line-shapes in **Figure 4-d**. The mathematical model used for fitting ITIC molecule is described in **SI 5**. The 0-0 transition energy for the first electronic excited state and the vibrational energy for the effective mode derived from fitting are $\varepsilon_{S_0 \to S_1} = 1.82\ \text{eV}$ and $\varepsilon_{\text{vib}} = 0.170\ \text{eV}\ (1371\text{cm}^{-1})$, respectively. These values are compatible with the DFT/TD-DFT simulated absorption (**Table 1**) and Raman spectra of ITIC (shown with dashed gray line in **Figure 3-g**). **Table S6** contains all the fitting parameters used to model ITIC absorption.

Since the successive peaks in the absorption spectrum of Y6 are not equi-energetic from each other, it is impossible to describe the spectrum utilizing a simple FC model with single vibronic progression. The TD-DFT results for Y6 in CF suggest that both $S_0 \to S_1$and $S_0 \to S_2$ transitions contribute to the absorption spectra. These transitions are predominantly $\text{HOMO} \to \text{LUMO}$ and $\text{HOMO} \to \text{LUMO} + 1$ for the first and second transition, respectively. The curved structure of Y6 allows for the nonzero TDM for the second electronic transition. Considering these results, the best FC model fit to the Y6 absorption spectra in CF is derived by superposition of two FC progressions ($S_0 \to S_1$and $S_0 \to S_2$) for a single conformation population, with two dominant vibrational modes (**Figure 4-e**, red solid lines and orange dashed lines) and three overtones (m=0,1,2) for each mode. **Figure 4-h** is the schematic of the FC model used to describe Y6 absorption spectrum in dilute solution. The model used for modeling Y6 molecule is described in **SI 6**. The excitation energies for the first and second electronic transitions derived from FC analyses are 1.69 and 2.08 eV, which are in agreement with the TD-DFT results (**Table 1**). The mean energy of effective vibrational modes derived from fitting are 154 meV (1242cm^{-1}) and 180 meV (1451cm^{-1}), respectively. These two modes are shown with two dashed gray lines in **Figure 3-h** which indicate a good relative agreement between FC analysis and simulated Raman spectrum (blue line) if an offset is considered between calculations and experiments. **Table S7** contains all the fitting parameters used to model Y6 absorption spectra.

The absorption spectrum of EH-IDTBR in CF consists of a broad peak at 1.89 eV with a shoulder at around 2.04 eV, which makes the FC modeling for this molecule quite challenging. The calculated dihedral PES scan of EH-IDTBR suggests a small potential barrier for rotation of the two dihedral angles at RT energies and indeed coexistence of multiple conformers of EH-IDTBR in the solution. Considering two different conformation populations with different energies (solid and dashed red lines in **Figures 4-i**), we could fit the absorption spectra of EH-IDTBR by an FC model with one effective vibrational mode. The fitting parameters for $\varepsilon_{S_0 \to S_1}$ are 1.87 and 2.03 eV for population **1** and **2**, respectively. Here, we consider different broadening for the two populations. The full-width-at-half-maximum (FWHM) for

the first population is 0.178 eV and 0.379 eV for the second population. The mean vibrational energy derived from FC analysis is 154 meV (1242cm^{-1}) shown in dashed gray line in **Figure 3-i** which is fairly in agreement with simulated Raman spectrum (blue line). All other fitting parameters are listed in **Table S8**. It is noteworthy that due to the broadening effects of these diverse vibrations, one can find multiple FC-based models that can describe the absorption spectra of EH-IDTBT. For instance, in **SI 7**, we show that considering only one population, but two different vibrational modes can also yield a fit that agrees with the experimental data. However, the large difference in broadening (0.178 eV versus 0.379 eV) would not be expected. Furthermore, the vibrational energies derived from this model are 135 meV (1088 cm^{-1}) and 220 meV (1774 cm^{-1}), which do not agree with the simulated Raman spectra and this particular model and fit has to be discarded. The combination of fitting and calculations allows to disentangle the electronic, conformation, and vibronic contributions even in the case when spectra are devoid of rich spectral features.

Table 1 Comparison between experimental values of excitation energies derived from FC analyses and TD-DFT results for ITIC, Y6 and EH-IDTBR molecules in CF calculated at the B3LYP/6-31G(d,p) level of theory.
*SE is the difference between calculated and experimentally measured (FC analysis) of excitation energies.

Molecule	Experiment (FC analysis) Energy(eV)	DFT Calculations B3LYP G(d,p) Energy(eV)	SE (eV)*
ITIC	1.82 ($s_0 \rightarrow s_1$)	1.77 ($s_0 \rightarrow s_1$)	0.05
Y6	1.69 ($s_0 \rightarrow s_1$)	1.71 ($s_0 \rightarrow s_1$)	-0.02
	2.08 ($s_0 \rightarrow s_2$)	2.05 ($s_0 \rightarrow s_2$)	0.03
EH-IDTBR	1.89 ($s_0 \rightarrow s_1$)	1.58 ($s_0 \rightarrow s_1$)	0.31

4. Discussion

The NF-SMA absorption spectra in this study feature different peak positions and/or broadening and cannot always be described by a simple FC model. The observed differences in the absorption spectra are indeed rooted in the structure-function properties and possible conformational disorder as discussed in the following. Our results show that the linear ITIC-like molecules with A-D-A structures mainly form one conformation in the solution, but due to heterogeneous broadening effects only one effective vibrational mode can be observed. The second group of SMAs, i.e., Y6-like structures, are locked into one confirmation, as it is shown by PES scans, Boltzmann analysis, and the presence of two effective vibrational modes. Details discussing the reasons why Y6-like molecules have one conformation population can be found in the **SI 8**. Moreover, the curved shape, i.e., the symmetry point group of these structures allows a second electronic transition that contributes to the spectra. In centrosymmetric systems like ITIC, with C_{2h} point group symmetry (centrosymmetric), the second electronic transition has a gerade symmetry that can only be excited with two photons from the symmetric ground state. However, in Y6 with C_{2v} symmetry point group (non-centrosymmetric), lack of an inversion center leads to second electronic excitation accessible via one-photon absorption[58]. In order to deconvolute the contribution of alkyl group sidechain and symmetry into the conformational uniformity, we consider two works done by Zhuohan Zhang et.al.,[59,60] in which the conformation locking effects on ITC6-IC and ITC6-4F are studied by introducing alkyl sidechain onto ITIC and IT-4F, respectively. For the case of ITIC like structures, we can use the estimate $s \sim \frac{I_{0-1}}{I_{0-0}}$ in dilute solution. Based on such an estimate from the reported absorption spectra of these structures in solution, we can conclude that by incorporating alkyl sidechains the HR factor (s) is slightly decreased. Assuming that the effective vibrational mode is similar for these structures, one can conclude that the reorganization energy of the structure with alkyl sidechain is reduced partially by introducing alkyl sidechains, however the symmetry of Y6 might have the largest contribution to its small reorganization energy. Moreover, smaller broadening effects in the absorption spectra of ITC6-IC and ITC6-4F indicate a higher conformational uniformity compared to the ITIC and IT-4F.

In the third group of SMAs, the presence of the extra π-bridge unit between the D unit and A units in the backbone, gives the molecule more degree of freedom to rotate around dihedral angles and adopt different conformations. A small PES barrier and smaller π-electron delocalization along the bridge results in higher conformational diversity in this group. The FC analysis of EH-IDTBR absorption spectra also confirms presence of two different confirmation populations with $\varepsilon_{S_0 \rightarrow S_1}$ equal to 1.87 and 2.03 eV for the first and second population, respectively.

For EH-IDTBR the experimental value of $\varepsilon_{S_0 \rightarrow S_1}$ is significantly larger than the TD-DFT results calculated for the optimized geometry at the B3LYP//6-31G(d,p) level of theory (**Table 1** , and **Table S5** for other functional). The large difference between the measured (1.89 eV) and simulated values (1.58 eV) for EH-IDTBR can be due to the presence of different conformations with different excitation energies. The conformations shorten the effective conjugation length and reduce the exciton delocalization/localization (**Figure S4**). Comparing these values with simulated values for $\varepsilon_{S_0 \rightarrow S_1}$ at different dihedral angles, it is evident that the EH-IDTBR molecules can be twisted in solution (**Figure S5**). For example, the calculated $\varepsilon_{S_0 \rightarrow S_1}$ for a twisted geometry with $\phi_2 = 90°$ is 1.87 eV with a 39% reduction in oscillator strength compared to 1.58 eV for the optimized extended geometry. This higher degree of conformation disorder generally increases the energetic disorder of a thin film, a critical parameter that controls tail states (DOS), non-radiative recombination, and V_{oc} losses[61–63].

In addition to revealing the number of contributing electronic and vibrational transitions, their corresponding energies, and conformation diversity, fitting an FC model to the absorption spectra can give information about the Huang Rhys (HR) parameter, which describes the electron-phonon coupling in the molecule[64] HR parameter s is defined as:

$$s = \frac{|V(Q)|}{\hbar\omega_{vib}} = \frac{\frac{1}{2}k\Delta Q^2}{\hbar\omega_{vib}} \qquad \textbf{(Eq-1)}$$

where V(Q) is the matrix element for exciton-phonon interaction and can be approximated by potential energy associated with a single harmonic oscillator with force constant k and displacement ΔQ [41,65]. Based on **Eq. 1**, the HR parameter gives the number of vibrational quanta involved in the excitation. Therefore, the intra-molecular reorganization energy during absorption of a photon can be given by [41]:

$$\lambda_{\mathrm{re,abs}} = s\hbar\omega_{vib} \quad \textbf{(Eq-2)}$$

Assuming similar HR parameter for the emissions, we can approximate the intra-molecular contribution to the Stokes shift by:

$$\lambda_{\mathrm{re}}^{\mathrm{intra}} = \lambda_{re,\mathrm{abs}} + \lambda_{\mathrm{re,em}} \approx 2s\hbar\omega_{vib} \quad \textbf{(Eq-3)}$$

Table 2 summarizes the HR parameter and $\lambda_{\mathrm{re}}^{\mathrm{intra}}$ derived from the FC analysis of the absorption spectra of each molecule. For a complex FC model with multiple electronic transitions (i) and vibrational modes (j) with energy $\boldsymbol{\omega_{vib,j}}$, the HR parameter for each electronic transition is:

$$s_i = \sum_j s_{i,j} \quad \textbf{(Eq-4)}$$

where $s_{i,j}$ is the HR parameters for j[th] vibrational mode in the i[th] electronic transition. The total intra-molecular contribution to the Stokes Shift for the i[th] electronic transition is:

$$\lambda_{re,i}^{intra} = \sum_j s_{i,j}\omega_{vib,j} \quad \textbf{(Eq-5)}$$

Based on these definitions, our results indicate that Y6 has the smallest total HR parameter (0.311) for the first electronic excitation compared to ITIC and EH-IDTBR (HR = 0.380 and 0.500, respectively), leading to smaller intra-molecular reorganization energy of $\lambda_{\mathrm{rel}}^{\mathrm{intra}} = 103$ meV, compared to 128 and 158 meV for ITIC and EH-IDTBR, respectively. We also performed DFT/TD-DFT simulation to calculate the Stoke shift of NF-SMAs using B3LYP/6-31G(d,p) (and wB97XD/6-31G(d,p) in **SI 11**). As shown in **Figure 5-a**, both FC analysis of experimental data and DFT/TD-DFT calculations predict similar trend for the molecular structure-reorganization energy correlation, indicating that Y6 has the smallest and EH-IDTBE the largest intra-molecular Stokes Shift. The small intra-molecular reorganization energy confirms higher rigidity of Y6 upon photoexcitation.

Table 2 HR parameters (s) and intra-molecular contribution to the Stokes Shift ($\Delta E_{\mathrm{rel}}^{\mathrm{intra}}$) derived from the FC analysis of absorption spectra.
* $\lambda_{\mathrm{re}}^{\mathrm{intra}} = \sum_j s_{i,j}\hbar\omega_{\mathrm{vib,j}}$, where $\hbar\omega_{\mathrm{vib},1} = 154\mathrm{meV}$ and $\hbar\omega_{\mathrm{vib},2} = 180\mathrm{meV}$.

Molecule	Definition of HR parameter: s	s	$\lambda_{\mathrm{rel}}^{\mathrm{intra}}$ (meV)
ITIC	For $S_0 \rightarrow S_1$: S_1	0.380	128
Y6	For $S_0 \rightarrow S_1$: $s_1 = s_{1,\omega_1} + s_{1,\omega_2}$	0.311	103*
	For $S_0 \rightarrow S_2$: $s_2 = s_{2,\omega_1} + s_{2,\omega_2}$	0.376	119
EH-IDTBR	For Population 1: s_{P_1}	0.500	154
	For Population 2: s_{P_2}	0.818	252

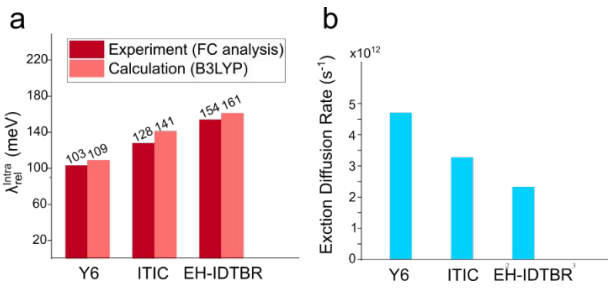

Figure 5 (a) Intra-molecular reorganization energy for NF-SMAs in this study derived from FC analysis of absorption spectra and DFT/TD-DFT calculation. (b) Exciton diffusion rate calculated based on Intra-molecular reorganization derived from FC analysis of Absorption spectra.

The intramolecular reorganization energy plays an important role in nonradiative recombination (NR) both in the exciton diffusion toward donor-acceptor interface and charge generation. In the case of exciton diffusion, the diffusion length of the exciton is:

$$L = \sqrt{ZD\tau} \quad \textbf{(Eq-6)}$$

where D and Z are diffusion coefficient and dimensionality of diffusion process. The diffusion time (τ) is determined by:

$$\tau = \frac{1}{k_{r,ex} + k_{nr,ex}} \quad \textbf{(Eq-7)}$$

where $k_{r,ex}$ and $k_{nr,ex}$ are the rate of radiative and non-radiative decays for the exciton. In the framework of Marcus electron-transfer theory, the $k_{nr,ex}$ is expressed by[19,27,66]:

$$k_{nr,ex} = \frac{V^2}{\hbar}\sqrt{\frac{\pi}{\lambda_{re}^{intra}k_BT}}\exp\left[-\frac{\lambda_{re}^{intra}}{4k_BT}\right] \quad \textbf{(Eq-8)}$$

where V denotes the electronic coupling element. Based on **Eq-8**, reducing the reorganization energy is a promising approach to improve the exciton diffusion length. Indeed, T. D. Anthopoulos et. al., showed that experimentally measured diffusion lengths for NF-SMA are related to the calculated reorganization energies[19]. Using **Eq-8**, we calculated the exciton transfer rate based on the reorganization energies derived from MFC analysis (**Figure 5-b**). We assumed a constant electronic element (40 meV) for all NF-SMA in this study, which is a good estimate based on the calculated values reported in literature[19]. **Figure 5-b** illustrates that the reduced reorganization energy of Y6 results in improvement of theoretical exciton diffusion rate by 43% and 100% compared to ITIC an EH-IDTBR. This underlines the importance of intramolecular reorganization energy on exciton diffusion length. In the solid state, the electronic coupling and diffusion might depend on the molecular packing.

In charge generation processes, the non-radiative recombination from the charge transfer (CT) state to ground state in an organic solar cell is related to the CT intramolecular reorganization energy (λ_{CT}). In this case, λ_{CT} is equal to the sum of the reorganization energies upon reduction of the donor cation and oxidation of the acceptor anion back to their neutral states[25,67]. Vandewal et al. showed that there exists an intrinsic link between nonradiative voltage losses (ΔV_{nr}) and electron–vibration couplings in CT states[22]. Also, Jenny Nelson et al., by exploring the effect of the different parameters on Voc, showed

that reducing λ_{CT} presents the best opportunity to increase Voc and, therefore, the PCE of the cells[68]. Lingyun Zhu et al., underlines the importance of the reorganization energy for achieving small energy loss in organic active materials. Their results also indicate that the calculated different reorganization energies during the photoelectric conversions have a similar trend as a function of molecular structure[21]. Therefore, the small λ_{rel}^{intra} of Y6 is indicating a larger exciton diffusion length and ΔV_{nr} compared to other NF-SMA in this study. Together these two factors contribute to the Y6 success in high performance OSCs with low voltage losses.

Interestingly, while the absorption spectra probe all the species in the system and provide information about population distributions, the emission spectra may not be a good probe for this purpose due to other contributing parameters like the migration of initial excitonic states to a lower state in polymers or aggregates in film, reorganization of solvent due to dipole moment interactions or formation of excited state dimers (excimer). For example, despite their absorption spectra, the emission spectra of all the NF-SMA solutions in this study (concentration of 0.02mg/ml in CF) are broad symmetric featureless spectra. Furthermore, increasing the concentration of the solutions from 0.02mg/ml to 0.1mg/ml doesn't change the shape (peak position and peaks ratio) of the absorption spectra of, but it introduces a drop in the Pl intensity and a shift toward smaller energies (**Figure S6**). This is due to the formation of excimers in the excited states since the absorption spectra don't change, while the emission is broadened, redshifted and quenched by increasing the concentration of NF-SMAs[69]. As a result, FC analysis of emission spectra without further complementary studies like time resolved Pl, temperatures-dependent PL or transient measurements does not provide reliable information about confirmation distributions.

5. Conclusion and Summary

has the smallest intra-molecular reorganization energy among the NF-SMAs in this study. This is due to the higher rigidity of Y6 upon photoexcitation. Small reorganization energy and low electronic disorder lead to larger exciton diffusion length and also smaller ΔV_{nr} which contribute to the success of Y6 in high performance OSCs with low voltage losses.

Our results indicate that that MFC analysis of RT absorption spectra alongside DFT/TD-DFT simulations can be an effective method to unravel the absorption spectra of SMAs and investigate the reorganization energy and the conformational and energetic diversity. This method avoids the complexity and challenges of other common optical method like Single Molecule Spectroscopy[70,71], in-situ Raman Spectroscopy and Transient Absorption Spectroscopy[72], and Temperature-Dependent and Time-Resolved Photoluminescence Spectroscopy[73]. Importantly, proper fitting allows accurate determination of the HR factor and reorganization energies that can be incorporated as a predictive measure for exciton diffusion length and ΔV_{nr} of the OSC materials in the OPV devices. RT UV-Vis analysis is experimentally much simpler than complementary measurements of reorganization energy. Also, the agreement between experiment and DFT calculations suggests that the latter can be used to design molecules *in-silico* with low reorganization energy and single conformations with low energetic disorder. Such molecular design can be extended to the materials use for organic devices other than OPV.

Author Contributions

Somayeh Kashani performed FC analysis, Quantum calculations and drafted the manuscript. Zhen Wang measured the absorption spectra, provided suggestions, and helped revise the manuscript. Chad Risko provided guidance and suggestions on Quantum calculations. All authors provided comments on the manuscript and contributed to the editing at all stages. Harald Ade directed the study.

Conflicts of interest

The authors declare no competing interests.

Acknowledgments

The work was supported by NSF grant DMR-1905770. Data acquired in part in the IMEKS facility at NCSU, supported by private foundations, the National Science Foundation and NC State University and maintained and supported by Prof. Castellano and Dr. Danilov. We acknowledge the computing resources provided by NC State University High Performance Computing Services Core Facility (RRID:SCR 022168). Fruitful related discussion about spectroscopy and exciton binding energy with Profs. N. Stingelin and C. Silva that motivated the current "back-to-basics" study are acknowledged.

References

1 Y. Lin, J. Wang, Z. G. Zhang, H. Bai, Y. Li, D. Zhu, and X. Zhan, Adv. *Mater*., 2015, **27**, 1170–1174.
2 K. Chong, X. Xu, H. Meng, J. Xue, L. Yu, W. Ma, Q. Peng, *Adv. Mater*., 2022, **34**, 2109516.
3 A. Karki, A. J. Gillett, R. H. Friend and T. Nguyen, *Adv. Energy Mater*., 2021, **11**, 2003441.
4 N. Liang, W. Jiang, J. Hou and Z. Wang, *Mater. Chem. Front.*, 2017, **1**, 1291–1303.
5 Z. Zhang, J. Yuan, Q. Wei and Y. Zou, *Front. Chem.,* 2018, **6**, 414.
6 J. Yuan, Y. Zhang, L. Zhou, G. Zhang, H.-L. Yip, T.-K. Lau, X. Lu, C. Zhu, H. Peng, P. A. Johnson, M. Leclerc, Y. Cao, J. Ulanski, Y. Li and Y. Zou, *Joule*, 2019, **3**, 1140–1151.
7 Q. Liu, Y. Jiang, K. Jin, J. Qin, J. Xu, W. Li, J. Xiong, J. Liu, Z. Xiao, K. Sun, S. Yang, X. Zhang and L. Ding, *Sci. Bull. (Beijing)*, 2020, **65**, 272–275.
8 A. Armin, W. Li, O. J. Sandberg, Z. Xiao, L. Ding, J. Nelson, D. Neher, K. Vandewal, S. Shoaee, T. Wang, H. Ade, T. Heumüller, C. Brabec and P. Meredith, *Adv. Energy Mater*., 2021, **11**, 2003570.
9 Z. Peng, L. Ye and H. Ade, *Mater. Horiz*., 2022, **9**, 577-606.

10 Q. Li and Z. Li, *Acc. Chem. Res*., 2020, **53**, 962–973.
11 G. Zhang, X.-K. Chen, J. Xiao, P. C. Y. Chow, M. Ren, G. Kupgan, X. Jiao, C. C. S. Chan, X. Du, R. Xia, Z. Chen, J. Yuan, Y. Zhang, S. Zhang, Y. Liu, Y. Zou, H. Yan, K. S. Wong, V. Coropceanu, N. Li, C. J. Brabec, J.-L. Bredas, H.-L. Yip and Y. Cao, *Nat. Commun.,* 2020, **11**, 3943.
12 H. Yao, L. Ye, J. Hou, B. Jang, G. Han, Y. Cui, G. M. Su, C. Wang, B. Gao, R. Yu, H. Zhang, Y. Yi, H. Y. Woo, H. Ade and J. Hou, Adv. Mater., 2017, 29, 1700254.
13 F. C. Spano, *Acc. Chem. Res.*, 2010, **43**, 429–439.
14 J. Clark, C. Silva, R. H. Friend and F. C. Spano, *Phys. Rev. Lett.,* 2007, **98**, 206406.
15 F. Panzer, M. Sommer, H. Bässler, M. Thelakkat and A. Köhler, *Macromolecules*, 2015, **48**, 1543–1553.
16 Y. Shi, Y. Chang, K. Lu, Z. Chen, J. Zhang, Y. Yan, D. Qiu, Y. Liu, M. A. Adil, W. Ma, X. Hao, L. Zhu and Z. Wei, *Nat. Commun*., 2022, **13**, 3256.
17 R. Duan, G. Han, L.-B. Qu and Y. Yi, *Mater. Chem. Front*., 2021, **5**, 3903–3910.
18 S. M. Menke, N. A. Ran, G. C. Bazan and R. H. Friend, *Joule*, 2018, **2**, 25–35.
19 Y. Firdaus, V. M. le Corre, S. Karuthedath, W. Liu, A. Markina, W. Huang, S. Chattopadhyay, M. M. Nahid, M. I. Nugraha, Y. Lin, A. Seitkhan, A. Basu, W. Zhang, I. McCulloch, H. Ade, J. Labram, F. Laquai, D. Andrienko, L. J. A. Koster and T. D. Anthopoulos, *Nat. Commun*., 2020, **11**, 5220.
20 G. Kupgan, X. K. Chen and J. L. Brédas, Mater. *Today Adv.*, 2021, **11**, 100154.
21 Y. Shi, Y. Chang, K. Lu, Z. Chen, J. Zhang, Y. Yan, D. Qiu, Y. Liu, M. A. Adil, W. Ma, X. Hao, L. Zhu and Z. Wei, *Nat. Commun*.,2022, **13**, 3256.
22 J. Benduhn, K. Tvingstedt, F. Piersimoni, S. Ullbrich, Y. Fan, M. Tropiano, K. A. McGarry, O. Zeika, M. K. Riede, C. J. Douglas, S. Barlow, S. R. Marder, D. Neher, D. Spoltore and K. Vandewal, *Nat. Energy*, 2017, **2**, 17053.
23 M. Azzouzi, J. Yan, T. Kirchartz, K. Liu, J. Wang, H. Wu and J. Nelson, *Phys. Rev. X*, 2018, **8**, 031055.
24 S. Liu, J. Yuan, W. Deng, M. Luo, Y. Xie, Q. Liang, Y. Zou, Z. He, H. Wu and Y. Cao, *Nat. Photonics*, 2020, **14**, 300–305.
25 X. K. Chen and J. L. Brédas, *Adv. Energy Mater*., 2018, **8**, 1702227.
26 S. Zeiske, C. Kaiser, P. Meredith and A. Armin, *ACS Photonics*, 2020, **7**, 256–264.
27 G. Han and Y. Yi, Adv. Theory Simul., 2019, 2, 1900067.
28 N. J. Hestand and F. C. Spano, *Chem. Rev*., 2018, **118**, 7069–7163.
29 M. De Jong, L. Seijo, A. Meijerink and F. T. Rabouw, *Phys. Chem. Chem. Phys*., 2015, **17**, 16959–16969.
30 H. Mustroph, Chem. Phys. Chem., 2016, 17, 2616–2629.
31 A. L. T. Khan, M. J. Banach and A. Köhler, *Synthetic Metals*, 2003, **139**, 905–907.
32 S. Wedler, A. Bourdick, S. Athanasopoulos, S. Gekle, F. Panzer, C. McDowell, T.-Q. Nguyen, G. C. Bazan and A. Köhler, *J. Mater. Chem. C Mater.,* 2020, **8**, 4944–4955.
33 D. Raithel, L. Simine, S. Pickel, K. Schötz, F. Panzer, S. Baderschneider, D. Schiefer, R. Lohwasser, J. Köhler, M. Thelakkat, M. Sommer, A. Köhler, P. J. Rossky and R. Hildner, *Proc. Natl. Acad. Sci.,* 2018, **115**, 2699–2704.
34 A. Köhler, S. T. Hoffmann and H. Bässler, *J. Am. Chem. Soc*., 2012, **134**, 11594–11601.
35 E. Rezasoltani, A. A. Y. Guilbert, J. Yan, X. Rodríguez-Martínez, M. Azzouzi, F. Eisner, S. M. Tuladhar, Z. Hamid, A. Wadsworth, I. McCulloch, M. Campoy-Quiles and *J. Nelson, Chem. Mater.,* 2020, **32**, 8294–8305.
36 F. Panzer, H. Bässler and A. Köhler*, J. Phys. Chem. Lett.,* 2017, **8**, 114–125.
37 J. Clark, C. Silva, R. H. Friend and F. C. Spano, *Phys. Rev. Lett*., 2007, **98**, 1–4.
38 N. J. Hestand and F. C. Spano, *Chem. Rev.*, 2018, **118**, 7069–7163.
39 C. Hellmann, F. Paquin, N. D. Treat, A. Bruno, L. X. Reynolds, S. A. Haque, P. N. Stavrinou, C. Silva and N. Stingelin, *Adv. Mater.,* 2013, **25**, 4906–4911.
40 W. Chen and Q. Zhang, *J. Mater. Chem. C. Mater.*, 2017, **5**, 1275–1302.
41 A. Köhler and H. Bässler, *Electronic Processes in Organic Semiconductors*, John Wiley & Sons, 2015.
42 Z. Zhang, J. Yuan, Q. Wei and Y. Zou, *Front. Chem*., 2018, **6**, 414.
43 J. Zhang, H. S. Tan, X. Guo, A. Facchetti and H. Yan, *Nat. Energy*, 2018, **3**, 720–731.
44 Z. Yin, S. Mei, P. Gu, H. Q. Wang and W. Song*, iScience*, 2021, **24**, 2021.
45 Y. Lin, Y. Firdaus, F. H. Isikgor, M. I. Nugraha, E. Yengel, G. T. Harrison, R. Hallani, A. El-Labban, H. Faber, C. Ma, X. Zheng, A. Subbiah, C. T. Howells, O. M. Bakr, I. McCulloch, S. De Wolf, L. Tsetseris and T. D. Anthopoulos, *ACS Energy Lett*., 2020, **5**, 2935–2944.
46 Q. Wei, W. Liu, M. Leclerc, J. Yuan, H. Chen and Y. Zou, *Sci. China Chem*., 2020, **63**, 1352–1366.
47 J. Zhao, C. Yao, M. U. Ali, J. Miao and H. Meng, *Mater. Chem. Front*., 2020, **4**, 3487–3504.
48 Z. Zhang, J. Yu, X. Yin, Z. Hu, Y. Jiang, J. Sun, J. Zhou, F. Zhang, T. P. Russell, F. Liu and W. Tang, *Adv. Funct. Mater.*, 2018, **28**, 1705095.
49 J. Yuan, Y. Zhang, L. Zhou, G. Zhang, H. L. Yip, T. K. Lau, X. Lu, C. Zhu, H. Peng, P. A. Johnson, M. Leclerc, Y. Cao, J. Ulanski, Y. Li and Y. Zou, *Joule*, 2019, **3**, 1140–1151.
50 Y. Chen, J. Liang, Y. Yu, L. Wang, C. Weng and P. Shen, *Org. Electron*., 2021, **89**, 106015.
51 Z. Wang, K. Huang, X. Chen, Y. Xu, Z. Xu, T. He, S. Yin, H. Qiu, M. Li and Q. Zhang, *J. Mater. Chem. C Mater.,* 2019, **7**, 14499–14503.
52 V. Barone and M. Cossi, *J. Phys. Chem. A*, 1998, **102**, 1995–2001.
53 M. Cossi and V. Barone, *J. Chem. Phys.,* 2000, **112**, 2427–2435.
54 M. Cossi, G. Scalmani, N. Rega and V. Barone, *J. Chem. Phys*., 2002, **117**, 43–54.
55 M. Cossi, N. Rega, G. Scalmani and V. Barone, *J. Comput. Chem*., 2003, **24**, 669–681.
56 J. Wu, J. Lee, Y. C. Chin, H. Yao, H. Cha, J. Luke, J. Hou, J. S. Kim and J. R. Durrant, *Energy Environ. Sci.,* 2020, **13**, 2422–2430.
57 S. Kedenburg, M. Vieweg, T. Gissibl and H. Giessen*, Opt. Mater. Express.*, 2012, **2**, 1588.
58 C. Zhong, D. Bialas, C. J. Collison and F. C. Spano*, J. Phys. Chem. C*, 2019, **123**, 18734–18745.
59 Z. Zhang, J. Yu, X. Yin, Z. Hu, Y. Jiang, J. Sun, J. Zhou, F. Zhang, T. P. Russell, F. Liu and W. Tang, *Adv Funct Mater*, 2018, **28**, 1705095.
60 Z. Zhang, X. Liu, J. Yu, H. Wang, M. Zhang, L. Yang, R. Geng, J. Cao, F. Du, F. Liu and W. Tang, *J. Mater. Chem. C*, 2019, **7**, 13279.
61 J. C. Blakesley and D. Neher, *Phys. Rev. B*, 2011, **84**, 075210.
62 M. Azzouzi, J. Yan, T. Kirchartz, K. Liu, J. Wang, H. Wu and J. Nelson, *Phys. Rev. X*, 2018, **8**, 031055.
63 C. McDowell, K. Narayanaswamy, B. Yadagiri, T. Gayathri, M. Seifrid, R. Datt, S. M. Ryno, M. C. Heifner, V. Gupta, C. Risko, S. Prakash Singh and G. C. Bazan, *J. Mater. Chem. A*, 2018, **6**, 383-394.

64 Y. Zhang, Journal of Semiconductors, 2019, 40, 091102.
65 H. Zhao and H. Kalt, *Phys. Rev. B,* 2003, **68**, 125309.
66 V. Stehr, R. F. Fink, B. Engels, J. Pflaum and C. Deibel, *J. Chem. Theory Comput.*, 2014, **10**, 1242–1255.
67 X.-K. Chen, V. Coropceanu and J.-L. Brédas, *Nat. Commun*., 2018, **9,** 5295.
68 J. L. Bricks, Y. L. Slominskii, I. D. Panas and A. P. Demchenko, *Methods Appl. Fluoresc*., 2017, **6**, 012001.
69 D. Kroh, F. Eller, K. Schötz, S. Wedler, L. Perdigón-Toro, G. Freychet, Q. Wei, M. Dörr, D. Jones, Y. Zou, E. M. Herzig, D. Neher and A. Köhler, *Adv. Funct. Mater*., 2022, 2205711, 2205711.
70 J. M. Lupton, Adv. Mater., 2010, 22, 1689–1721.
71 F. Schindler, J. M. Lupton, J. Feldmann and U. Scherf, *Proc. Natl. Acad. Sci*., 2004, **101,** 14695–14700.
72 K. Roy, S. Kayal, V. Ravi Kumar, A. Beeby, F. Ariese and S. Umapathy, *J. Phys. Chem. A*, 2017, **121**, 6538–6546.
73 Y. Z. Shi, K. Wang, S. L. Zhang, X. C. Fan, Y. Tsuchiya, Y. T. Lee, G. Le Dai, J. X. Chen, C. J. Zheng, S. Y. Xiong, X. M. Ou, J. Yu, J. S. Jie, C. S. Lee, C. Adachi and X. H. Zhang, *Angewandte Chemie*, 2021, **60**, 25878–25883.